Geosci. Instrum. Method. Data Syst. Discuss., 2, 539–561, 2012
www.geosci-instrum-method-data-syst-discuss.net/2/539/2012/
doi:10.5194/gid-2-539-2012

Discussions Geoscientific Instrumentation Methods and Data Systems

Geo-neutrinos

L. Ludhova

Istituto Nazionale di Fisica Nucleare, via Celoria 16, 20133 Milano, Italy

Received: 23 July 2012 – Accepted: 24 July 2012 – Published: 3 August 2012

Correspondence to: L. Ludhova (livia.ludhova@mi.infn.it)

Published by Copernicus Publications on behalf of the European Geosciences Union.

Abstract

Geo-neutrinos, electron anti-neutrinos produced in β-decays of naturally occurring radioactive isotopes in the Earth, are a unique direct probe of our planet's interior. After a brief introduction about the Earth (mostly for physicists) and the very basics about the neutrinos and anti-neutrinos (mostly for geologists), I describe the geo-neutrinos' properties and the main aims of their study. An overview of the latest experimental results obtained by KamLand and Borexino experiments is provided. A short overview of future perspectives of this new inter-disciplinary field is given.

1 Introduction

The introduction is divided into three parts. First, the structure, composition, and sources of information about the Earth are described. It is a short summary meant mostly for physicists. Secondly, the basic physics of neutrinos and anti-neutrinos, relevant for the geo-neutrino studies are described. This part is meant mostly for geologists. The last part of the introduction finally describes the geo-neutrinos, their properties, and the importance of their study.

1.1 The Earth (mostly for physicists)

It is assumed that the Earth was created via accretion as an homogeneous object. The metallic core (3500 km radius) was the first to separate from the silicate primordial mantle which further differentiated into the current mantle (3000 km thickness) and the crust (5 to 75 km). The Fe-Ni metallic core with up to $\sim$ 10 % admixture of lighter elements, has a temperature range from 4100 to 5800 K. Its central part, inner core with the radius $\sim$ 1300 km is solid due to high pressure. The 2200 km thick outer core is liquid and has a key role in the geo-dynamo process generating the Earth's magnetic field. The D'' layer is a core-mantle boundary, a 200 km thick seismic discontinuity of unclear origin. The lower mantle (2000 km) with a temperature gradient from 600 to

GID
2, 539–561, 2012

3700 K is solid, but viscose on long time scales. It is involved in the convection driving the movement of tectonic plates with a speed of few centimeters per year. A transition zone in the depth of 400–600 km is a seismic discontinuity due to mineral recrystallization. The upper mantle contains viscose astenosphere on which are floating the lithospheric tectonic plates. These comprise the uppermost, rigid part of the mantle and the crust of two types: oceanic and continental. The continental crust (30 km average thickness) has the most complex history being the most differentiated and heterogeneous, consisting of igneous, metamorphic, and sedimentary rocks. The oceanic crust (5–10 km) is created along the mid-oceanic ridges where the basaltic magma differentiates from the partially melting mantle. A schematic profile of the Earth structure can be found in Fig. 1.

Information about the Earth's interior composition has insofar come exclusively from indirect probes. Geophysics, studying the propagation of mechanical waves through the Earth, constrains the density profile and the phase state. Geochemistry has limited sources of direct data as well and develops models of the Earth bulk composition based on indirect information. The deepest drill hole ever made (12 km, Kola, Russia) represents enormous technical difficulties, but is negligible with respect to the Earth radius of $\sim$6400 km. Some geological processes bring the deep rocks to the surface (volcanism, obduction, xenolites ...) but their chemical composition can be altered during the transport and the deep mantle is completely unreachable. Similar trends of relative abundances of chemical elements in meteorites and in the Sun's photosphere indicate that the Solar system developed from a chemically homogeneous nebula. Assuming these trends for the primordial Earth as well as rock melting trends which produced the current rocks, the Bulk Silicate Earth (BSE) model was developed, describing the composition of the primitive mantle. The BSE model therefore describes the composition of the silicate Earth, the mean composition of the Earth after the metallic core separation and before the crust-mantle differentiation. Several authors developed such models, e.g. Turcotte and Schubert (2002), Anderson (2007), Palme and O'Neill (2003), Allegre et al. (1995), McDonoough et al. (1995), Lyubetskaya and Korenaga (2007), and Javoy

GID
2, 539–561, 2012

et al. (2010). The predictions of the absolute abundances of the long-lived radioactive elements producing geo-neutrinos differ up to a factor of 2–3, while the predictions of their relative proportions are in a much better agreement within 10 %.

The total terrestrial surface heat flux is deduced from the temperature-gradient measurements along ~ 40 000 drill holes distributed around the world. It is important to note that these drill holes are not distributed homogeneously, they are concentrated mostly on the continental crust, while almost missing in the hottest regions along the mid-ocean ridges. Using these temperature gradient data, geophysical models typically conclude that the present surface heat flux is 47 ± 2 TW (Davies and Davies, 2010). This conventional view has been challenged by an alternative flux estimate of 31 ± 1 TW (Hofmeister and Criss, 2004) and other authors predict 44 TW (Pollack et al., 1993). Such big discrepancies indicate that some systematic errors or model assumptions are out of the control.

There are several possible sources contributing to the total terrestrial surface heat flux and the radiogenic heat is generally considered as a main contribution to the total heat budget. The main long-lived radioactive elements producing this radiogenic heat are ^{238}U, ^{232}Th, and ^{40}K. The range of the BSE models predicting the Th, U, and K abundances translates to radiogenic heat contributions of 12–30 TW (crust + mantle). Typically, based on geophysical calculations, parameterized convection models of the mantle require higher radiogenic heat contributions (~ 70 % of the total heat flux) in order to describe the Earth's cooling history in terms of a balance of forces between thermal dissipation and mantle viscosity. Consequently, a geochemist's view of the Earth predicts that its budget of heat producing elements in the BSE are up to a factor of ~ 3 lower than the models predicted by geophysicists. Thus, the relative contribution of the radioactive power to the total planetary heat flux is poorly known. No contribution is expected from the core. Thorium and uranium are refractory lithophile elements and contribute equally ~ 80 % of the total radiogenic heat production of the Earth, while the remaining fraction is due to ^{40}K, a volatile element (assuming Th/U ~ 4 and K/U ~ 10 000) (Wurm et al., 2012). During mantle melting and because of their chemistry

GID
2, 539–561, 2012

and size, K, Th, and U are quantitatively partitioned into the melt and depleted from the mantle. Thus, the continental crust, has over geologic time, been enriched in these elements and has a sizable fraction (about half) of the planet's inventory, producing radiogenic power of 7.3 ± 1.2 TW (Rudnick and Gao, 2003). The main unknown remain the abundances of the long-lived radioactive elements and the radiogenic heat produced in the mantle.

It is possible that additional heat sources contribute to the total surface heat flux (estimated based on the temperature gradient measurements). Such additional heat might originate from accretion, gravitational contraction, latent heat from phase transitions, or from a (rather exotic) nuclear reactor in the core/core-mantle boundary (Herndon, 1996) or presence of ^{40}K in the metallic core. It can be concluded, that systematic errors in both geochemical and geophysical models are not very well known and the validity of several assumptions on which they are based is not proven.

1.2 Neutrinos and anti-neutrinos (mostly for geologists)

Neutrinos (ν) and their anti-particles, anti-neutrinos ($\bar{\nu}$), are the fundamental elementary particles belonging to the family of leptons. In contrast to charged leptons (electron, muon, and tau particles with negative electric charge and their positively charged anti-particles), they have no electric charge, so they do not interact via electromagnetic forces. All leptons do not interact via strong interactions. Neutrinos and anti-neutrinos, being neutral leptons, can interact only via weak interactions, making the probability of their interaction along their passage through matter very rare. The so called cross-section of their weak interactions with matter is of the order of 10^{-45} cm^2. It means, that neutrinos and anti-neutrinos, once detected, can bring to the observer undisturbed information about the region of their production. The same low probability of interaction makes these particles extremely difficult to detect and often huge multi-ton detectors placed in underground laboratories in order to shield them from the cosmic radiation are required for (anti-)neutrino detection.

GID
2, 539–561, 2012

Both neutrinos and anti-neutrinos exist in three types, so called flavors: electron, muon, and tau. Each flavor is a linear combination of 3 so called mass eigenstates, labeled simply 1, 2, and 3, each flavor in characteristics proportions of 3 mass eigenstates. The dominant neutrino flux on the Earth comes from the electron flavor neutrinos produced in the nuclear reactions powering the Sun: the flux of about $10^{10}\,\mathrm{cm}^{-2}\,\mathrm{s}^{-1}$ with energies below 11 MeV. Neutrinos are usually detected via elastic scattering off electrons. The dominant sources of electron anti-neutrino fluxes on the Earth surface is the Earth itself (geo-neutrinos with energies below 3.5 MeV) and the nuclear power plants producing anti-neutrinos with energies up to 10 MeV. Geo-neutrinos are electron flavor anti-neutrinos, produced in β-decays of ^{40}K and of several nuclides in the chains of long-lived radioactive isotopes ^{238}U and ^{232}Th, which are naturally present in the Earth. Their typical flux on the Earth's surface is about $10^{6}\,\mathrm{cm}^{-2}\,\mathrm{s}^{-1}$. Electron flavor anti-neutrinos are detected via the inverse neutron β-decay reaction,

$$\bar{\nu}_{\mathrm{e}} + p \rightarrow e^{+} + n, \tag{1}$$

with a kinematic threshold of 1.806 MeV.

Both neutrinos and anti-neutrinos are very light particles and therefore they propagate with the velocity very close that of light. During their passage, the neutrino and/or anti-neutrino is represented as a mixtures of 3-mass eigenstates with periodically evolving proportions. Therefore, the (anti-)neutrino which was produced in an interaction characterizing it as being of a certain flavor can be later on detected as an (anti-)neutrino of the same or of a different flavor. For electron anti-neutrinos, the probability to be detected again as electron anti-neutrinos oscillates according to (Fiorentini et al., 2012):

$$P_{\mathrm{ee}} = \cos^4\theta_{13}\left(1 - \sin^2(2\theta_{12})\sin^2\left(\Delta m^2_{12}L/4E\right)\right) + \sin^4\theta_{13}, \tag{2}$$

where θ_{12} and θ_{13} are the mixing parameters, so called mixing angles, Δm^2_{12} is a difference of the squares of masses of mass eigenstates 1 and 2, while E is the anti-neutrino

GID
2, 539–561, 2012

energy and L is the source-detectors distance. As we can see, for an anti-neutrino of a certain energy, the P_{ee} changes with distance L. For a 3 MeV anti-neutrino (about the end-point of the geo-neutrino's spectrum and the peak energy of reactor neutrinos), the oscillation length is of ~ 100 km. Therefore, for geo-neutrinos originating from a continuous source of few thousands of kilometers (the Earth mantle and crust), the oscillation pattern cannot be distinguished on the energy spectrum of detected geo-neutrinos and one can consider only the reduction of the total flux by $(1 - P_{ee})$ with $P_{ee} = 0.551 \pm 0.015$ (Fiorentini et al., 2012). In the two flavor approximation considering $\theta_{13} = 0$ the P_{ee} is increased by about 0.009. For considering the spectral shape of reactor anti-neutrinos the oscillation pattern has to be taken into account.

1.3 Geo-neutrinos

Geo-neutrinos (geo-$\bar{\nu}_e$), electron anti-neutrinos ($\bar{\nu}_e$) are produced in β-decays of ^{40}K and of several nuclides in the chains of long-lived radioactive isotopes ^{238}U and ^{232}Th, which are naturally present in the Earth:

$$^{238}\mathrm{U} \rightarrow {}^{206}\mathrm{Pb} + 8\alpha + 8e^- + 6\bar{\nu}_e + 51.7\,\mathrm{MeV} \quad (3)$$

$$^{232}\mathrm{Th} \rightarrow {}^{208}\mathrm{Pb} + 6\alpha + 4e^- + 4\bar{\nu}_e + 42.8\,\mathrm{MeV} \quad (4)$$

$$^{40}\mathrm{K} \rightarrow {}^{40}\mathrm{Ca} + e^- + \bar{\nu}_e + 1.32\,\mathrm{MeV}. \quad (5)$$

The Earth shines in geo-neutrinos with a flux of about $10^6\,\mathrm{cm}^{-2}\,\mathrm{s}^{-1}$. It is important to note that the ratio of the released radiogenic heat and the geo-neutrino flux is in a well fixed and known ratio. Therefore, it is in principle possible to determine the amount of the radiogenic heat contributing to the total terrestrial surface heat flux (Urey ratio) by measuring the geo-neutrino flux. By measuring the geo-neutrino flux at different locations through the globe, in different geological settings and/or by being able to identify the incoming direction of detected geo-neutrinos, it might be possible to:

GID
2, 539–561, 2012

- study the distribution of radioactive elements within the Earth, to determine their abundances in the crust and in the mantle;
- determine if there are any radioactive elements in the Earth's core;
- understand if the mantle composition is homogeneous or not;
- test, validate and discriminate among different BSE models;
- exclude or confirm the presence of the geo-reactor in the core;
- determine the so called Urey ratio by measuring the radiogenic heat flux, an important parameter for both geochemistry and geophysics.
- to study the bulk U and Th ratio in the sillicate Earth, an important parameter for geochemistry which could shed light on the process of the Earth's formation;

We can see that geo-neutrinos can be used as a unique direct probe of the Earth interior, not accessible by any other means. All these informations could be important data used as inputs for many geological, geophysical, and geochemical models describing such complex processes as the mantle convection, movement of tectonic plates, geodynamo (the process of the generation of the Earth's magnetic field), the process of the Earth formation etc.

The energy spectrum of geo-neutrinos extends to about 3.3 MeV. They are detected via the inverse neutron β-decay reaction described above, see Eq. (1) which has a kinematic threshold of 1.806 MeV. The cross section of this interaction as a function of anti-neutrino energy is well known and can be found in (Strumia and Vissani, 2003). Unfortunately, all geo-neutrinos produced in the decay of ^{40}K are below this threshold and we are able to detect only the tail of the ^{238}U and ^{232}Th geo-neutrinos. Geo-neutrinos from the ^{232}Th chain have the end point of their energy spectrum at about 2.25 MeV while those from the ^{238}U chain extend up to 3.3 MeV. Ideally, this spectral feature could be used in order to measure the U and Th ratio in the Earth. It is important to recall, that the relative proportions of the elements abundances are much

GID
2, 539–561, 2012

better known than their absolute abundances. Therefore, by measuring the absolute abundances of ^{238}U and ^{232}Th, the absolute abundance of ^{40}K can be deduced with a better precision.

2 Latest geo-neutrino experimental results

There are only two running experiments able to measure geo-neutrinos: Borexino placed at Laboratori Nazionali del Gran Sasso in central Italy and KamLand in Kamioka mine in Japan. Both experiments are large volume scintillator detectors placed in the underground in order to shield from cosmic rays. Both experiments detect geo-neutrinos via the inverse beta decay reaction, see Eq. (1) in which anti-neutrino interacts with a free proton (hydrogen nucleus) and a positron and a neutron are the reaction products. The positron promptly comes to rest and annihilates emitting two 511 keV γ-rays, yielding a prompt event, with a visible energy E_{prompt} directly correlated with the energy of incident anti-neutrino $E_{\bar{\nu}_e}$:

$$E_{\text{prompt}} = E_{\bar{\nu}_e} - 0.782\,\text{MeV}. \quad (6)$$

The free neutron emitted is typically captured on protons with a mean time of $\tau \sim 200$–$250\,\mu$s, resulting in the emission of a 2.22 MeV de-excitation γ-ray, which provides a coincident delayed event. The characteristic time and spatial coincidence of prompt and delayed events offers a clean signature of $\bar{\nu}_e$ detection.

The known $\bar{\nu}_e$ sources are geo-$\bar{\nu}_e$ and reactor $\bar{\nu}_e$, while atmospheric and supernova relic $\bar{\nu}_e$'s give a negligible contribution. A detailed analysis of the expected reactor anti-neutrino rate is necessary for both experiments. The determination of the expected signal from reactor $\bar{\nu}_e$'s requires the collection of the detailed information on the time profiles of the thermal power and nuclear fuel composition for nearby reactors. In Japan there are many nuclear power plants and in addition KamLand detector was constructed to measure reactor anti-neutrinos, so it is placed close to the reactor. Therefore, the reactor anti-neutrino background for geo-neutrino measurement

GID
2, 539–561, 2012

was quite high in this experiment. To the contrary, in Italy there are no nuclear power plants (the mean reactor distance is of approximately 1000 km), so the reactor anti-neutrino flux in Borexino is up to a factor of 7 lower then in KamLand. In addition, since neutrinos are detected via elastic scattering off electrons of the scintillator, there is no coincidence tag to may distinguish neutrino interactions from the signals due to the natural radioactivity background. Therefore, the extreme radio-purity is a must for Borexino which in fact succeeded to decrease the internal radioactivity background to unprecedented low levels. Therefore, the other important backgrounds for geo-neutrino measurements, random coincidences and (α, n) interactions in which α's are mostly from the ^{210}Po decay, are strongly suppressed in Borexino. To the contrary, KamLand has an advantage of bigger target mass since it features about 1 kton of liquid scintillator while Borexino "only" 280 t. For both detectors the scintillator is placed in the very core of the detector and it is shielded by a layer of the buffer liquid (mineral oil in KamLand and quenched scintillator in Borexino). The scintillator volume is viewed by an array of about 2000 photomultipliers. The scintillation light isotropically propagates from the interaction point outwards. The number of hit photomultipliers is a measure of energy deposited in the detector. The position of the interaction point can be determined via the time-of-flight measurement of detected scintillation photons. The time of each trigger is flagged by a gps time stamp. In both detectors the scintillator and buffer containing vessels are further surrounded by a tank filled with ultra-pure water, called Outer Detector. This medium serves both as a passive shield against external gamma's and neutrons as well as an active muon Cherenkov detector equipped with about 200 photomultipliers detecting Cherenkov light produced by cosmic muons traversing water. The schemes of the Borexino and KamLand detectors are shown in Figs. 2 and 3, respectively.

Borexino and KamLand are placed in very different geological environments and are also very far from each other. Borexino is placed on a continental crust while KamLand on oceanic crust. The measurements from both experiments are therefore

GID
2, 539–561, 2012

complementary and probing different geological settings, and they could shed light on the hypothesis of a homogeneous vs heterogeneous mantle.

The first experimental indication of a geo-neutrino measurement ($\sim 2.5\sigma$ C.L.) was reported by the KamLand collaboration (Araki et al., 2005; Abe et al., 2008). The observation of geo-neutrinos at 99.997 % C.L. was then achieved by both Borexino (Bellini et al., 2010) and KamLand (Gando et al., 2011). The observed energy spectra of the prompt candidates are showed in Figs. 4 and 5, respectively.

Borexino detected in total 21 candidates in 537.2 days of live time and in the energy range up to the end point of the reactor anti-neutrino spectrum. The result of an unbinned maximum likelihood fit gives the number of detected geo-neutrinos $N_{geo} = 9.9^{+4.1}_{-3.4}$ and the number of reactor anti-neutrinos $N_{react} = 10.7^{+4.3}_{-3.4}$. The Th:U ratio was fixed to the chondritic value of 3.9. The contribution of other background results negligible. Figure 6 shows the allowed regions for N_{geo} and N_{react} at 1, 2, and 3σ C.L. These results hint at a higher rate for geo-$\bar{\nu}_e$ than the BSE from Fiorentini et al. (2007) predicts, but the uncertainty prevents any conclusions.This Borexino measurement rejects the hypothesis of an active geo-reactor of composition as in Herndon (1996) in the Earth's core with a power above 3 TW at 95 % C.L.

KamLand detected 841 anti-neutrino candidates in the geo-neutrino energy window between 0.9 MeV and 2.6 MeV. The best fit with the Th:U ratio fixed to the chondritic value of 3.9 results in the number of detected geo-neutrinos $N_{geo} = 106^{+29}_{-28}$. The $\Delta\chi^2$-profile from the fit to the total number of geo-neutrino events is shown in Fig. 7. The best fit is in agreement with the prediction of the BSE model from Enomoto et al. (2007), but other models cannot be firmly excluded yet.

KamLand performed a combined analyses of the KamLand and Borexino results, which are summarized in Fig. 8. They find that decay of ^{238}U and ^{232}Th together contribute $20.0^{+8.8}_{-8.6}$ TW to the Earth's surface heat flux. They adopt the estimation of the total heat flux from ^{40}K of 4 TW. They conclude, that the radiogenic heat contributes about half to the total Earth's heat flux and that other heat sources or the Earth's

GID
2, 539–561, 2012

primordial heat are contributing to the total heat budget. The fully radiogenic, homogeneous hypothesis is therefore excluded at 97.2 % C.L.

3 Future perspectives

The two geo-neutrino measurements opened a door towards a new field. It was proved that geo-neutrinos can be detected and that we, as a mankind, have a new tool how to learn new things about our planet. In order to find definitive answers to the questions correlated to the radiogenic heat and abundances of radiogenic elements, more data is needed. Both Borexino and KamLAND will continue to take data in the near future. The earthquake disaster in Japan in March 2012 caused the reactor power plants in Japan to be switched off and some of them will be restarted after a thorough campaign of tests. The strong reduction of the reactor anti-neutrino background could help in improving the future geo-neutrino measurement of KamLand. In addition it would be important to construct larger volume detectors in order to increase the number of detected geo-neutrinos and so improve the precision of the flux measurement. Results from different detector sites placed at different geological settings is a key point for understanding, for example, if the Earth mantle composition and heat distributions are homogeneous or not. Answers to questions like what is the bulk-Earth U versus Th ratio, is it the same like in meteorites can help in better understanding of the process of Earth formation and the distribution of elements in the Solar system. A new generation of experiments using liquid scintillators is either under the design or even construction process. SNO+ at Sudbury mine in Canada (Chen et al., 2006), having 1000 t of target, is in an advanced construction phase. The site is located on an old continental crust and the signal from reactor anti-neutrinos is about twice as the one at Gran Sasso. A new ambitious project to construct a 50 000 t detector is called LENA (Wurm et al., 2012). Among the most probable sites are Pyhäsalmi in Finland or Fréjus in France. This experiment could detect at the order of 1000 geo-neutrinos per year. A few percent precision of the total flux measurement could be reached within the first couple of

GID
2, 539–561, 2012

few years. The individual contribution of the U and Th geo-neutrino flux could be determined as well. An interesting project of 5000 t underwater experiment is HanoHano (Learned, 2007) planned to be placed on the oceanic crust (Hawaii). Due to the thin oceanic crust, the mantle contribution to the total geo-neutrino flux should be dominant. Therefore, this measurement would provide the most direct information about the mantle. This forthcoming project together with the currently running experiments could be a starting point of a network useful to understand the Earth heat distribution.

References

Abe, S. et al.: KamLAND collaboration: Measurement of Neutrino Oscillation Parameters with KamLAND, Phys. Rev. Lett., 100, 221803, doi:10.1103/PhysRevLett.100.221803, 2008. 549

Alimonti, G. et al.: Borexono collaboration: The Borexino detector at the Laboratori Nazionali del Gran Sasso, Nucl. Instrum. Meth. A, 600, 568–593, 2009. 555

Allégre, C. J., Poirier, J. P., Humler, E., and Hofmann, A. W.: The chemical composition of the Earth, Earth Planet. Sc. Lett., 134, 515–526, 1995. 541

Anderson, D. L.: The New Theory of the Earth, Cambridge University Press, 400 pp., 1997. 541

Araki, T. et al.: KamLAND collaboration: Experimental investigation of geologically produced antineutrinos with KamLAND, Nature, 436, 499–503, 2005. 549

Bellini, G. et al., Borexino collaboration: Observation of geo-neutrinos, 2010, Phys. Lett. B, 687, 299–304, 2010. 549, 557, 559

Chen, M. J.: Geo-neutrinos in SNO+, Earth Moon Planets, 99, 221–228, 2006. 550

Davies, J. H. and Davies, D. R.: Earth's surface heat flux, Solid Earth, 1, 5–24, doi:10.5194/se-1-5-2010, 2010. 542

Enomoto, S., Ohtani, E., Inoue, K., and Suzuki, A.: Neutrino geophysics with KamLAND and future prospects, Earth Planet Sc. Lett., 258, 147–159, 2007. 549, 560

Fiorentini, G., Lissia, M., and Mantovani, F.: Geo-neutrinos and Earth's interior, Phys. Rep., 453, 117–172, doi:10.1016/j.physrep.2007.09.001, 2007. 549, 559

Fiorentini, G., Fogli, G. L., Lisi, E., Mantovani, F., and Rotunno, A. M.: Mantle geoneutrinos in KamLAND and Borexino, arXiv:1204.1923, submitted, 2012. 544, 545

GID
2, 539–561, 2012

Gando, A. et al.: KamLAND collaboration: Partial radiogenic heat model for Earth revealed by geoneutrino measurements, Nat. Geosci., 4, 647–651, doi:10.1038/ngeo1205, 2011. 549, 558, 560, 561
Herndon, J. M.: Substructure of the inner core of the Earth, P. Natl. Acad. Sci. USA, 93, 646–648, 1996. 543
Hofmeister, A. M. and Criss, R. E.: Earth's heat flux revised and linked to chemistry, Tectonophysics, 395, 159–177, 2004. 542
Javoy, M., Kaminski, E., Guyot, F., Andrault, D., Sanloup, C., Moreira, M., Labrosse, S., Jambon, A., Agrinier, P., Davaille, A., and Jaupart, C.: The chemical composition of the Earth: Enstatite chondrite models, Earth Planet. Sc. Lett., 293, 259–268, 2010. 541
Learned, J. G., Dye, S. T., and Pakvasa, S.: Hanohano: A Deep Ocean Anti-Neutrino Detector for Unique Neutrino Physics and Geophysics Studies, in: Proceedings of the XII International Workshop on Neutrino Telescopes, 6–9 March 2007, edited by: Baldo Ceolin, M., Venice, 235–269, 2007. 551
Lyubetskaya, T. and Korenaga, J.: Chemical composition of Earth's primitive mantle and its variance: 2. Implications for global geodynamics, J. Geophys. Res., 112, B03211, doi:10.1029/2005JB004223, 2007. 541
McDonough, W. F. and Sun, S.-S.: The composition of the Earth, Chem. Geol., 120, 223–253, 1995. 541
Palme, H. and O'Neill, H. S. C: Cosmochemical Estimates of Mantle Composition, Treat. Geochem., 2, 1–38, 2003. 541
Pollack, H. N., Hurter, S. J., and Johnson, J. R.: Heat flow from the Earth's interior: Analysis of the global data set, Rev. Geophys., 31, 267–280, 1993. 542
Rudnick, R. L. and Gao, S.: The Composition of the Continental Crust, Treat. Geochem., 3, 1–64, 2003. 543
Strumia, A. and Vissani, F.: Precise quasielastic neutrino/nucleon cross section, Phys. Lett. B, 564, 42–54, 2003. 546
Suekane, F. for the KamLAND collaboration: Review KamLAND, Prog. Part. Nucl. Phys., 57, 106–126, 2006. 556
Turcotte, D. and Schubert, G.: Geodynamics, Cambridge University Press, 472 pp., 2002. 541
Wurm, M., Beacom, J. F., Bezrukov, L. B., Bick, D., Blümer, J., Choubey, S., Ciemniak, Ch., D'Angelo, D., Dasgupta, B., Derbin, A., Dighe, A., Domogatsky, G., Dye, S., ELiseev, S., Enquist, T., Erykalov, A., von Feilitzsch, F., Fiorentini, G., Fischer, T., Göger-Neff, M., Grabmayr,

GID
2, 539–561, 2012

P., Hagner, C., Hellgartner, D., Hissa, J., Horiuchi, S., Janka, H. T., Jaupart, C., Jochum, J., Kalliokoski, T., Kayunov, Al, Kuusiniemi, P., Lachenmaier, T., Lazanu, I., Learned, J. G., Lewke, T., Lombardi, P., Lorenz, S., Lubsandorzhiev, B., Ludhova, L., Loo, K., Maalampi, J., Mantovani, F., Marafini, M., Maricic, J., Marrodan Undagoitia, T., McDonough, W. F., Miramonti, L., Mirizzi, Al., Meindel, Q., Mena, O., Möllenberg, R., Muratova, V., Nahnhauer, R., Nesterenko, D., Novikov, Y. N., Nuijten, G., Oberauer, L., Pakvasa, S., Palomates-Ruiz, S., Pallavicini, M., Pascoli, S., Patzak, T., Peltoniemi, J., Potzel, W., Raiha, T., Raffelt, G. G., Ranucci, G., Razzaque, S., Rammukainen, K., Sarkamo, J., Sinev, V., Spiering, Ch., Stahl, A., THorne, F., Tippmann, M., Tonazzo, A., Trzaska, W. H., Vergados, J. D., Wiesbusch, Ch., and Winter, J.: The next-generation liquid-scintillator neutrino observatory LENA, Astro. Phys., 35, 685–732, doi:10.1016/j.astropartphys.2012.02.011, 2012. 542, 550

GID
2, 539–561, 2012

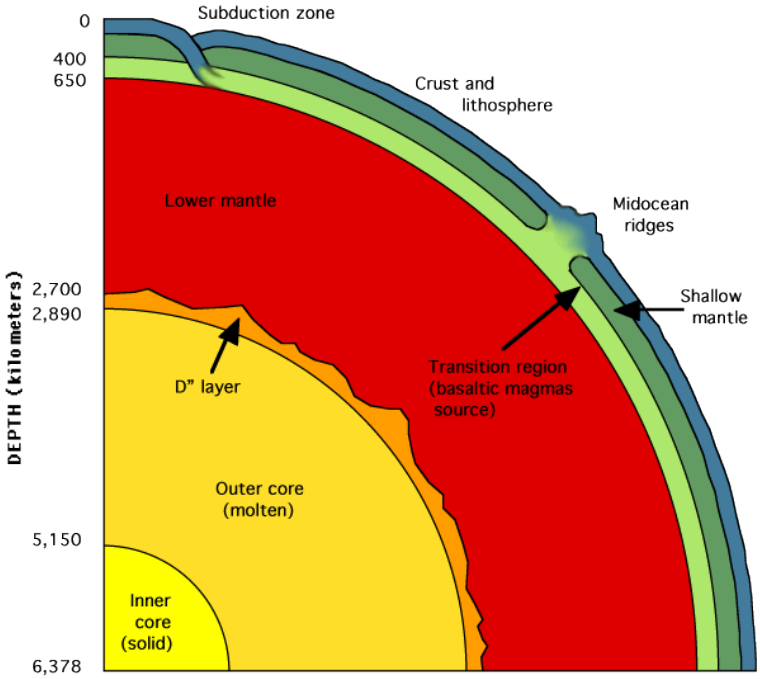

Fig. 1. A schematic profile of the Earth structure (from http://www.homepages.ucl.ac.uk/~ucfbdxa/resint.htm). Details in the text.

GID
2, 539–561, 2012

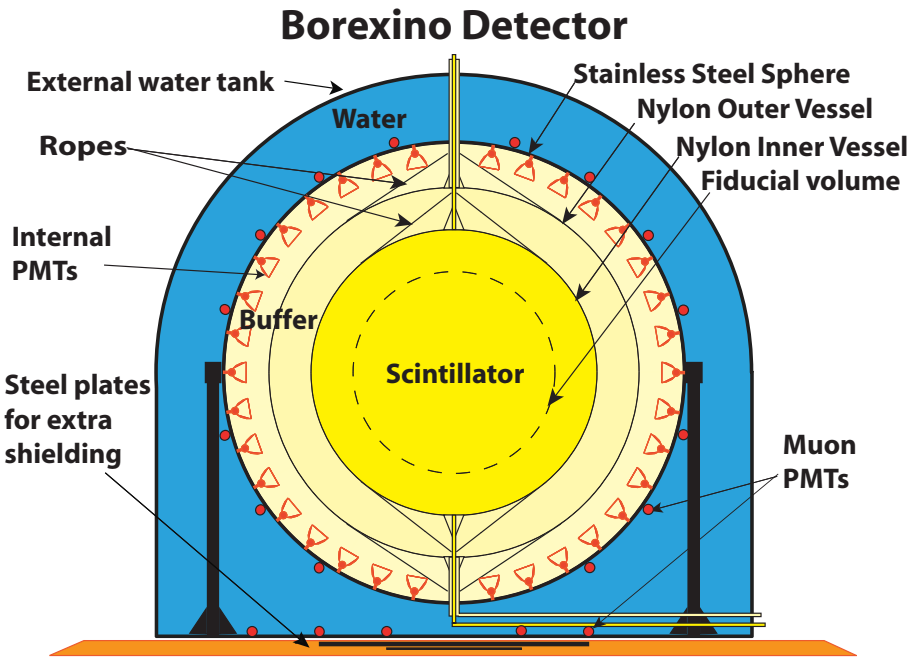

Fig. 2. Schematic view of the Borexino detector (Alimonti et al., 2010).

GID
2, 539–561, 2012

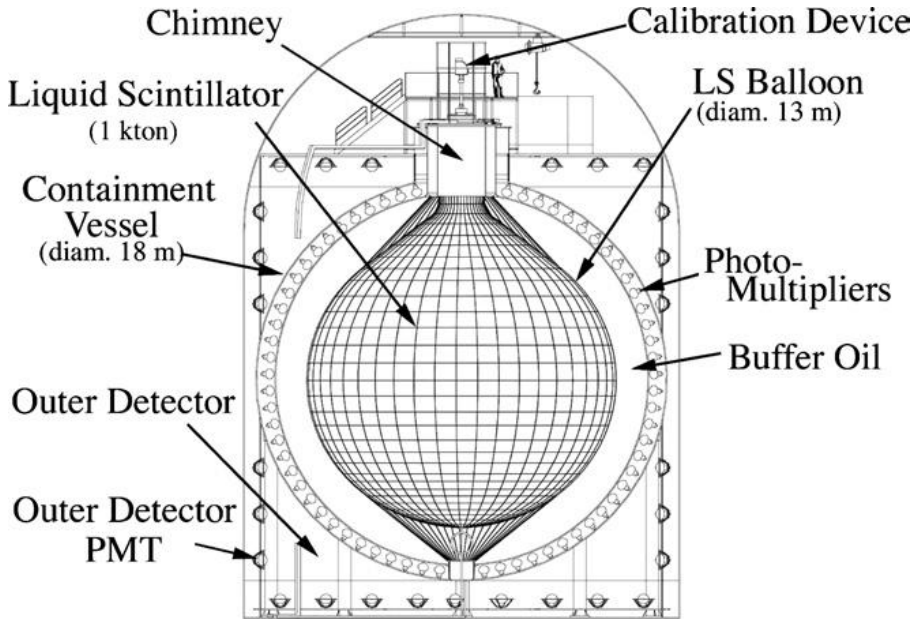

Fig. 3. Schematic view of the KamLand detector (Suekane et al., 2006).

GID
2, 539–561, 2012

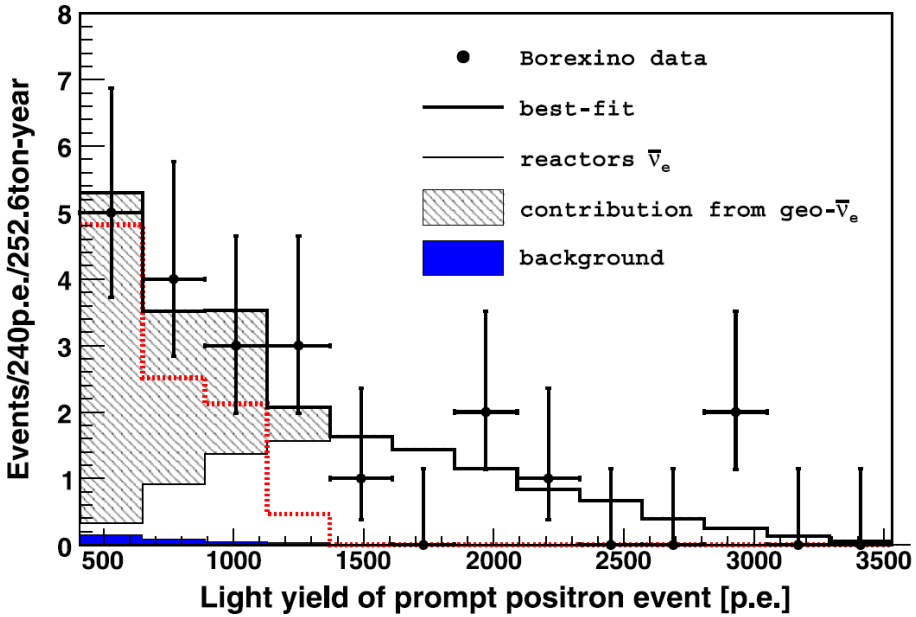

Fig. 4. Borexino data and fit (Bellini et al., 2010): light yield spectrum for the positron prompt events of the 21 $\bar{\nu}_e$ candidates and the best-fit (solid thick line). The small filled area is the background. Thin solid black and dotted red lines: reactor- and geo-$\bar{\nu}_e$ signal from the fit, respectively. The darker area isolates the contribution of the geo-$\bar{\nu}_e$ in the total signal. The conversion from p.e. to energy is approximately 500 p.e./MeV.

GID
2, 539–561, 2012

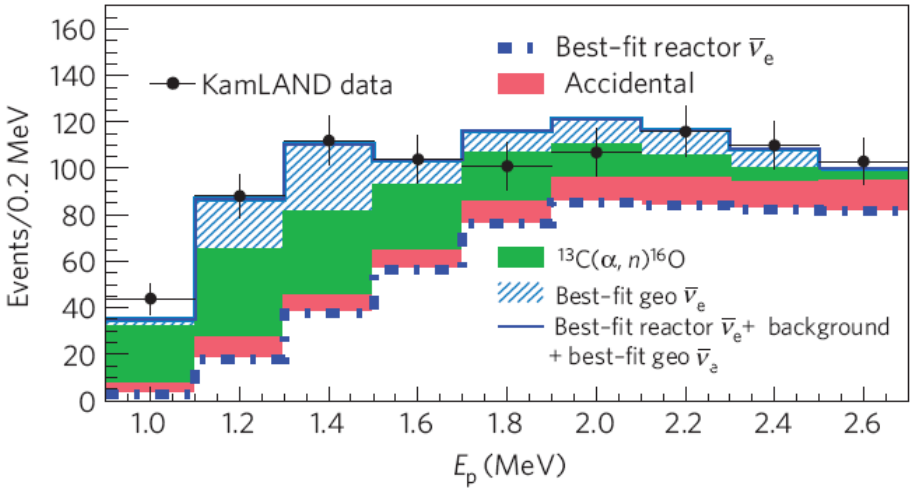

Fig. 5. KamLand data and fit (Gando et al., 2011): prompt energy spectrum of low-energy anti-neutrino spectrum. The histograms indicate the backgrounds, whereas the best fit (including geo-neutrinos) is shown in blue.

GID
2, 539–561, 2012

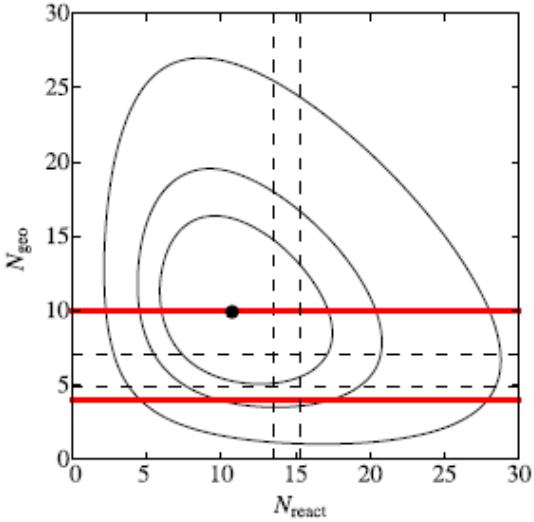

Fig. 6. Borexino contour plot (Bellini et al., 2010): allowed regions for N_{geo} and N_{react} at 68 %, 90 %, and 99.73 % C.L. Vertical dashed lines: 1σ range about the expected N_{react} (expected in presence of neutrino oscillations). Horizontal dashed lines: range for N_{geo} predictions based on the BSE model in Fiorentini et al. (2007). Horizontal solid red lines: predictions of the Fully Radiogenic and Minimal Radiogenic Earth (only the crust contribution considered) models.

GID
2, 539–561, 2012

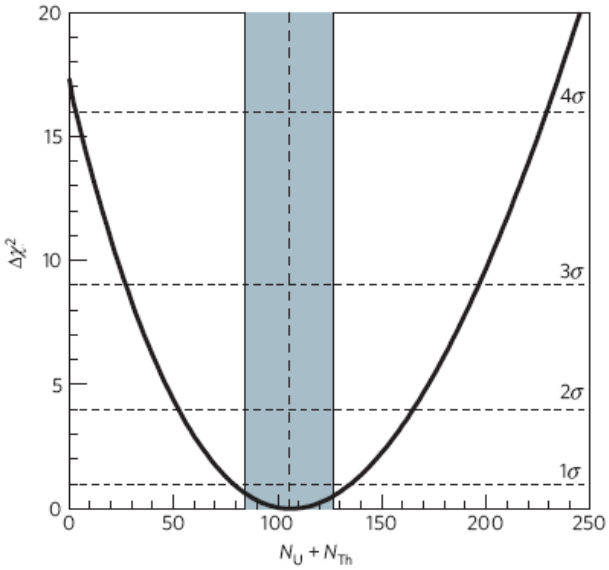

Fig. 7. KamLand results (Gando et al., 2011): $\Delta\chi^2$-profile from the fit to the total number of geo-neutrino events. The BSE model from Enomoto et al. (2007) prediction is represented by the shaded bend.

GID
2, 539–561, 2012

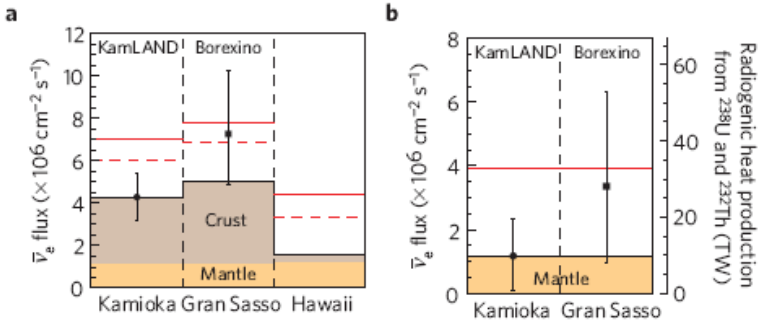

Fig. 8. Borexino and KamLand combined analysis from Gando et al. (2011): **(a)** measured geo-neutrinos flux at KamLand and Borexino sites, and expected fluxes at these sites and Hawaii. The red lines represent fully radiogenic models under different assumptions. **(b)** Measured geo-neutrinos flux after subtracting the estimated crustal contribution. No modeling uncertainties are shown. The solid red line indicates the fully radiogenic model.

GID
2, 539–561, 2012